Journal of Photochemistry & Photobiology, A: Chemistry 411 (2021) 113200

Contents lists available at ScienceDirect

Journal of Photochemistry & Photobiology, A: Chemistry

journal homepage: www.elsevier.com/locate/jphotochem

Enhanced photo-ablation effect of positively charged phthalocyanines-detonation nanodiamonds nanoplatforms for the suppression of *Staphylococcus aureus* and *Escherichia coli* planktonic cells and biofilms

Yolande Ikala Openda, Tebello Nyokong *

Institute for Nanotechnology Innovation, Department of Chemistry, Rhodes University, Makhanda 6140, South Africa

ARTICLE INFO

Keywords:
Detonation nanodiamonds
Chalcone phthalocyanines
Biofilms
Planktonic
Photodynamic antimicrobial therapy

ABSTRACT

Photodynamic antimicrobial therapy (PACT) is a powerful technic recommended to eliminate life-threatening pathogens that cause localized and superficial infections as pathogens cannot develop resistance to it. For this reason, new positively charged chalcone substituted zinc (**3a**) and indium (**4a**) metalated phthalocyanines (Pcs) were synthesized and were π-π interacted with detonation nanodiamonds (DNDs) nanoparticles to form new water soluble nanoplatfoms **3a**@DNDs and **4a**@DNDs. The conjugates generated high singlet oxygen quantum yields (Φ_Δ) in water (1% DMSO, used for PACT studies) with values of 0.46 and 0.47 for **3a**@DNDs and **4a**@DNDs, respectively. Hence, they were tested for PACT against biofilms of *S. aureus* and *E. coli*, as well as their planktonic cells. The quaternized Pcs alone **3a** and **4a** as well as their nanoconjugates **3a**@DNDs and **4a**@DNDs were effective PACT agents with $\log_{10}$ CFU > 9 for *E. coli* and *S. aureus*. The quaternized derivatives were found to have higher ability to completely suppress both planktonic and biofilms of *S. aureus* and *E. coli in vitro*. Therefore, they could be used as appropriate photosensitive agents.

1. Introduction

Up to 60 % of severe infection cases leading to deaths globally are attributed to bacterial biofilms. Free pathogenic bacteria cells that adhere to a living or inert surface tend to form a bacterial biofilm structure [1,2]. It is much more difficult to eradicate pathogenic bacteria living within a biofilm as they easily develop resistance to the available antibiotic drugs and treatments [3–5]. Additionally, bacteria in biofilms can tolerate 10–1000 times higher dosage of antibiotics than their planktonic forms (free bacteria cells) [6]. Therefore, the major challenge remain to develop new antibiofilm approaches to fight against bacteria biofilms, either by biofilm structure disruption or suppression of biofilm [7]. Amongst many techniques based on the generation of singlet oxygen, there is photodynamic antimicrobial chemotherapy (PACT).

The photodynamic effect consist of a non-toxic photosensitizer (PS) that is activated by visible light of appropriate wavelength in the presence of oxygen leading to the production of reactive oxygen species (ROS) including singlet oxygen that can cause cell death [8,9]. Concentration, nature and spectral properties of a PS are crucial in the efficacy of PACT [8,10]. PACT does not target a single site in bacteria, unlike conventional antibiotics. ROS target various bacterial cell structures and different metabolic pathways [11]. Thus, bacteria do not readily develop resistance to PACT [12].

Several studies have also indicated that the photoinactivation of Gram-negative bacteria (*i.e. E. coli*) is quite challenging because of the complexity in the composition of their cell wall as compared to Gram-positive bacteria (*i.e. S. aureus*) [13]. Therefore, it is agreed that a good PS should also combine characteristics such as hydrophilicity and positive charge(s) for attachment towards negatively charged bacterial cell walls, but also to prevent aggregation in aqueous medium and improve cell uptake [14–17]. Metallophthalocyanines (MPcs) are known PACT photosensitizers for planktonic cells and biofilms [18–20]. Increasing the number of positive charges on the substituents enhances the extent of phthalocyanine binding to gram-negative bacteria such as *E. coli* [21]. Thus, the development of new polycationic phthalocyanines is needed [22] as they show successful PACT activities and high affinity to the bacteria cells.

Hence in this work, we synthesize new pyridine chalcone

* Corresponding author.
E-mail address: t.nyokong@ru.ac.za (T. Nyokong).

https://doi.org/10.1016/j.jphotochem.2021.113200
Received 14 September 2020; Received in revised form 1 February 2021; Accepted 6 February 2021
Available online 12 February 2021

tetrasubstituted zinc and indium Pcs and their quaternized (positively charged) Pc derivatives. Chalcone substituted MPcs have been reported for photodynamic therapy (PDT) of cancer, which is similar to PACT [23,24] and other applications [25,26]. The use of chalcone substituted MPcs for PACT is reported in this work for the first time. In addition, the pyridine chalcone substituent on MPcs allows for quaternization, making the complexes water soluble. Chalcone derivatives are known for their antibacterial activities [27], hence they can enhance PACT activities of the MPcs, by synergetic effect. In addition, chalcones are known for their vascular disrupting effect in PDT, which destroy the tumor's neovasculature, leading to tumor starvation and subsequently to tumor death by necrosis [24].

To further extend the range of nanotechnology applications in biomedical fields, we used detonation nanodiamonds (DNDs) to make nanoconjugates with MPcs. DNDs have been used recently in fighting infectious diseases and biofilm formation and have proven to be a possible alternative to common antimicrobials [5]. Nanodiamonds have been widely used in many biomedical fields such as bactericides, wound dressing agents and as components in different drug delivery matrices, *etc*. [28]. The presence of π electrons on DNDs allows for π-π interactions with other π containing molecules such as MPcs, and this is applied in this work.

Thus, the objectives of the current work is to prepare a nanoplatform composed of water soluble and positively charged Pcs and DNDs that can display inhibition activity against planktonic cells and biofilms of both gram-positive bacteria (*e.g. S. aureus*) and gram-negative bacteria (*e.g. E. coli*) using photodynamic antimicrobial therapy method.

2. Experimental

Materials and equipment items used in this work can be found in the Supporting Information (SI).

2.1. Synthesis

2.1.1. (E)-1-(4-hydroxyphenyl)-3-(pyridin-4-yl)prop-2-en-1-one (1), Scheme 1

A solution of 4-hydroxyacetophenone (1 g, 7.3 mmol) and 4-pyridinecarbaxaldehyde (0.7867 g, 7.3 mmol) in ethanol (20 mL) was added drop-wise to a stirred solution of 30 % KOH cooled at 0 °C in an ice bath under argon atmosphere. The reaction mixture was kept at room temperature for 24 h and the completion of the reaction was monitored by thin layer chromatography (TLC) using hexane:ethylacetate (2:1, v/v). At the completion, the reaction mixture was poured into iced water and adjusted to neutral pH with 1 M HCl then the precipitate was filtered out. The yellow powder product was obtained by recrystallization from ethanol yielding 65.23 % of the desired product.

IR (UATR-TWO™) ν max/cm^{-1}: 3140 (OH), 3050 (Ar C—H and intermolecular H bonds), 2917

(Alph C—H), 1658 (C═O), 1586 (C═C), 1570 (C═N), 1509–1419 (C—C). ^{1}H NMR (600 MHz, DMSO- d_6): δ (ppm): 10.58 (bs, 1H, —OH), 8.65 (*d*, *J* =6 Hz, 2 H), 8.12 (*d*, *J* =16 Hz, 1 H), 8.09 (*d*, *J* =9 Hz, 2 H), 7.81 (*d*, *J* =6 Hz, 2 H), 7.61 (*d*, *J* =16 Hz, 1 H), 6.93 (*d*, *J* =6 Hz, 2 H). ^{13}C NMR (600 MHz, DMSO- d_6): δ (ppm): 187.3, 162.9, 150.6, 142.3, 140.1, 131.7, 128.9, 126.8, 122.7 and 115.8. MALDI TOF MS *m/z*: Calcd: 225.24 Found: $[M+H]^+$= 226.39.

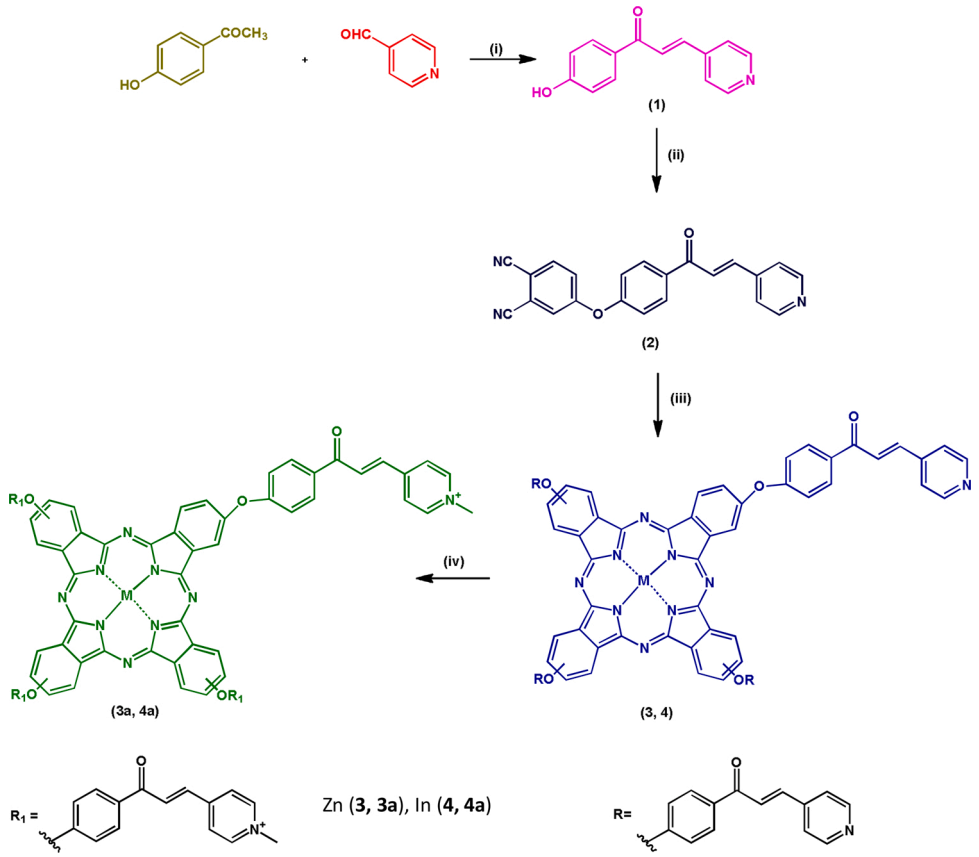

Scheme 1. The synthesis route of (**1**), the dinitrile compound (**2**) and novel phthalocyanines (**3, 3a, 4** and **4a**). Reaction conditions: (i): KOH, EtOH, at 25 °C, Ar; (ii): anhydrous K_2CO_3, anhydrous dry DMF, 4-nitrophthalonitrile, 60 °C, Ar; (iii): dry DMAE (for **3** and quinoline for **4**), DBU and anhydrous zinc acetate or indium chloride at 160 °C, Ar; (iv): dry DMF, acetone and excess CH_3I at reflux.

2.1.2. Synthesis of (E)-4-(4-(3-(pyridin-4-yl)acryloyl)phenoxy) phthalonitrile (2)

4-Nitrophthalonitrile (0.369 g, 2.1 mmol) and compound **1** (0.400 g, 1.8 mmol) were dissolved in 15 mL of *N,N*- dimethylformamide (DMF) in a round-bottom flask and stirred under argon atmosphere. K_2CO_3 (0.368 g, 2.7 mmol) was added then the stirring was continued for 24 h at 60 °C. The reaction mixture was afterwards poured into 50 mL iced water. The obtained orange solid was filtered out and recrystallized in ethanol to obtain **2**. Yield: 0.5175 g (83 % yield). IR (UATR-TWO™) ν max/cm^{-1}: 3068 (Ar C—H and intermolecular H bonds), 2937 (Aliph C═H), 1667 (C═O), 1583 (C═C), 1538 (C═N), 2231 (C≡N), 1486–1360 (C—C), 1287–1166 (*Asym.*, Ar—O—Ar), 1098 (*Sym.*, Ar—O—Ar), 802. ^{1}H NMR (600 MHz, DMSO-d_6): δ (ppm): 8.93 (*d*, *J* =8 Hz, 2 H), 8.88 (*d*, *J* =9 Hz, 2 H), 8.34 (*d*, *J* =8 Hz, 1 H), 8.03 (*d*, *J* =16 Hz, 1 H), 7.95 (*s*, 1 H), 7.92 (*d*, *J* =16 Hz, 1 H), 7.44 (*d*, *J* =8 Hz, 2 H), 7.37 (*d*, *J* =8 Hz, 1 H) and 7.26 (*d*, *J* =9 Hz, 2 H). ^{13}C NMR (600 MHz, DMSO- d_6): δ (ppm): 186.7, 162.8, 154.2, 151.8, 143.6, 131.6, 130.8, 130.7, 130.5, 129.2, 124.5, 1223, 116.3, 115.5, 115.4, 111.8 and 111.1. MALDI TOF MS *m/z*: Calcd: 351.36; Found: $[M+H]^+ = 352.14$.

2.1.3. Phthalocyanines (3, 4), Scheme 1

Under argon atmosphere, the dinitrile compound **2** (0.250 g, 0.72 mmol) was dissolved in dry dimethylaminoethanol (DMAE, 3 mL) and anhydrous zinc acetate (0.065 g, 0.354 mmol) was added for phthalocyanine **3.** For phthalocyanine **4**, compound **2** (0.250 g, 0.712 mmol) was dissolved in dry quinoline (3 mL) and anhydrous indium chloride (0.472 g, 2.13 mmol) was added. Following this, a few drops of DBU were added in each reaction mixture and these were brought to reflux for 24 h. After completion, the mixtures were cooled to room temperature, then ethanol was added and the reaction mixtures were further stirred for 1 h. The obtained green crude products were collected under centrifugation and were purified on silica gel using chloroform: ethanol (9:1) as an eluting solvent mixture.

ZnPc (**3**): Yield: 0.187 g (36 %). IR (UATR-TWO™) ν max/cm^{-1}: 3055 (Ar—H), 2923–2855 (Aliph C—H), 1721 (C═O), 1583–1490 (C═C, C═N), 1413–1362 (C—C), 1228–1164 (*Asym.*, Ar—O—Ar), 1086 (*Sym.*, Ar—O—Ar), 832. ^{1}H NMR (600 MHz, DMSO- d_6): δ (ppm): 8.97–8.95 (*m*, 8H, ArH-pyridine ring); 8.90 (*d*, 8H, ArH); 8.25 (*d*, 2H, ArH-Pc ring); 8.20 (*d*, 2H, ArH-Pc ring); 8.03 (*d*, 4H, CH═CH); 7.96–7.92 (*m*, 8H, ArH-Pc ring and CH═CH); 7.46–7.44 (*dd*, 8H, ArH-pyridine ring), 7.39 (*d*, 4H, ArH-Pc ring) and 7.28 (*d*, 8H, ArH). MALDI TOF MS *m/z*: Calcd: 1470.81; Found: $[M+H]^+ = 1471.88$. Anal. Calc. for [$C_{88}H_{52}N_{12}O_8Zn$] (%): C, 71.86; H, 3.56; N, 11.43; Found (%): C, 71.81; H, 3.59; N, 11.49.

InPc (**4**): Yield: 0.300 g (27 %). IR (UATR-TWO™) ν max/cm^{-1}: 3056 (Ar-H), 2923–2856 (Aliph C—H), 1722 (C═O), 1583–1491 (C═C, C═N), 1413–1362 (C—C), 1228–1164 (Asym., Ar—O—Ar), 1087 (Sym., Ar—O—Ar), 832. ^{1}H NMR (600 MHz, DMSO- d_6): δ (ppm): 8.97–8.95 (*m*, 8H, ArH-pyridine ring); 8.90 (*d*, 8H, ArH); 8.26 (*d*, 2H, ArH-Pc ring); 8.20 (*d*, 2H, ArH-Pc ring); 8.03 (*d*, 4H, CH═CH); 7.96–7.92 (*m*, 8H, ArH-Pc ring and CH═CH); 7.46–7.44 (*dd*, 8H, ArH-pyridine ring), 7.39 (*d*, 4H, ArH-Pc ring) and 7.28 (*d*, 8H, ArH). MALDI TOF MS *m/z*: Calcd: 1555.70; Found: $[M]^+ = 1555.26$. Anal. Calc. for [$C_{88}H_{52}ClInN_{12}O_8$] (%): C, 67.94; H, 3.37; N, 10.80; Found (%): C, 67.96; H, 3.39; N, 10.84.

2.1.4. Quaternized phthalocyanines (3a and 4a), Scheme 1

The quaternization of the Pcs was done following a procedure described in literature with slight modifications [29] as follows: **3** (0.050 g, 0.034 mmol) or **4** (0.050 g, 0.032 mmol) were each dissolved in dry DMF (3 mL)/acetone (5 mL) solvent mixture. Excess iodomethane (4 mL) was added to the solution. The reaction mixtures were heated at reflux temperature for 72 h. The green products were precipitated out with hot acetone and collected by centrifugation. Afterwards the products were washed with acetone, tetrahydrofuran (THF) and diethyl ether and dried under reduced pressure.

ZnPc (**3a**): Yield: 0.048 g (92 %). IR (UATR-TWO™) ν max/cm^{-1}: 3055 (Ar-H), 2928–2855 (Aliph C—H), 1721 (C═O), 1583–1490 (C═C, C═N), 1411–1362 (C—C), 1228–1164 (*Asym.*, Ar—O—Ar), 1086 (*Sym.*, Ar—O—Ar), 832. ^{1}H NMR (600 MHz, DMSO- d_6): δ (ppm): 8.97–8.95 (*m*, 8H, ArH-pyridine ring); 8.90 (*d*, 8H, ArH); 8.25 (*d*, 2H, ArH-Pc ring); 8.20 (*d*, 2H, ArH-Pc ring); 8.03 (*d*, 4H, CH═CH); 7.96–7.92 (*m*, 8H, ArH-Pc ring and CH═CH); 7.46–7.44 (*dd*, 8H, ArH-pyridine ring), 7.39 (*d*, 4H, ArH-Pc ring); 7.28 (*d*, 8H, ArH) and 2.90 (*s*, 12H, CH_3). MALDI TOF MS *m/z*: Calcd: 1530.95; Found: $[M+H]^+ = 1531.99$. Anal. Calc. for [$C_{92}H_{64}N_{12}O_8Zn$] (%): C, 72.18; H, 4.21; N, 10.98; Found (%): C, 72.26; H, 4.19; N, 10.94.

InPc (**4a**): Yield: 0.05 g (98 %). IR (UATR-TWO™) ν max/cm^{-1}: 3056 (Ar-H), 2925–2856 (Aliph C—H), 1722 (C═O), 1583–1491 (C═C, C═N), 1413–1362 (C—C), 1228–1164 (*Asym.*, Ar—O—Ar), 1087 (Sym., Ar—O—Ar), 832. ^{1}H NMR (600 MHz, DMSO- d_6): δ (ppm): 8.97–8.95 (*m*, 8H, ArH-pyridine ring); 8.90 (*d*, 8H, ArH); 8.25 (*d*, 2H, ArH-Pc ring); 8.20 (*d*, 2H, ArH-Pc ring); 8.03 (*d*, 4H, CH═CH); 7.96–7.92 (*m*, 8H, ArH-Pc ring and CH═CH); 7.46–7.44 (*m*, 8H, ArH-pyridine ring), 7.39 (*d*, 4H, ArH-Pc ring); 7.28 (*d*, 8H, ArH) and 2.90 (*s*, 12H, CH_3). MALDI TOF MS *m/z*: Calcd: 1615.84; Found: $[M+H]^+ = 1616.39$. Anal. Calc. for [$C_{92}H_{64}ClInN_{12}O_8$] (%): C, 68.38; H, 3.39; N, 10.40; Found (%): C, 68.28; H, 3.30; N, 10.46.

2.1.5. Conjugation of zinc phthalocyanines to detonation nanodiamonds (DNDs), Scheme 2

The nanoconjugation of the Pc complexes as well as their quaternized derivatives to DNDs nanoparticles to form Pcs@DNDs nanoconjugates was done through π-π stacking interactions accordingly to a previously reported procedure [30] as follows: Pc **3** (0.010 g, 0.0068 mmol) or Pc **4** (0.010 g, 0.0064 mmol) or Pc **3a** (0.010 g, 0.0065 mmol) or Pc **4a** (0.010 g, 0.0062 mmol) were each dissolved in dry DMSO (3 mL), then DNDs (5 mg) were added to each solution. The mixtures were sonicated for 4 h, followed by stirring for 96 h at room temperature. The resulting products were precipitated out by centrifugation and washed repetitively with ethanol for the non-quaternized Pcs and with acetone and THF for the quaternized Pcs, to remove the unreacted Pcs and DNDs, then the products were air dried. The formed nanoconjugates are represented as **3**@DNDs, **3a**@DNDs, **4**@DNDs and **4a**@DNDs.

2.2. Photophysicochemical properties

Fluorescence (Φ_F) quantum yields for both the Pcs and their nanoconjugates were determined by comparative methods as defined in literature with equations shown in the supporting information. ZnPc dissolved in DMSO with reported values of $\Phi_F = 0.2$ [31] was used as standard.

Singlet oxygen quantum yields (Φ_Δ, were determined using ZnPc (in DMSO, $\Phi_\Delta = 0.67$ [32]) or AlPcSmix (in 1% DMSO aqueous media, $\Phi_\Delta = 0.42$ [32]) as references for non-quaternized and quaternized products, respectively. Diphenylisobenzofuran (DPBF) and anthreacene-910-bis-methylmalonate (ADMA) were used as singlet oxygen chemical quenchers in DMSO and aqueous media respectively. DPBF and ADMA photobleaching effects were respectively monitored at 417 nm and 378 nm, respectively.

2.3. PACT studies

2.3.1. Antibacterial assays on planktonic cells

The gram positive *Staphylococcus aureus* and gram negative *Escherischia coli* bacterial planktonic cells were prepared for PACT studies as previously reported in literature [29,33,34] as follows: the inoculation of an aliquot of each bacterial species was aseptically done in 5 mL of freshly prepared nutrient broth, followed by an overnight cultivation in an incubator with shaker at 37 °C. The individual bacterial inocula in the

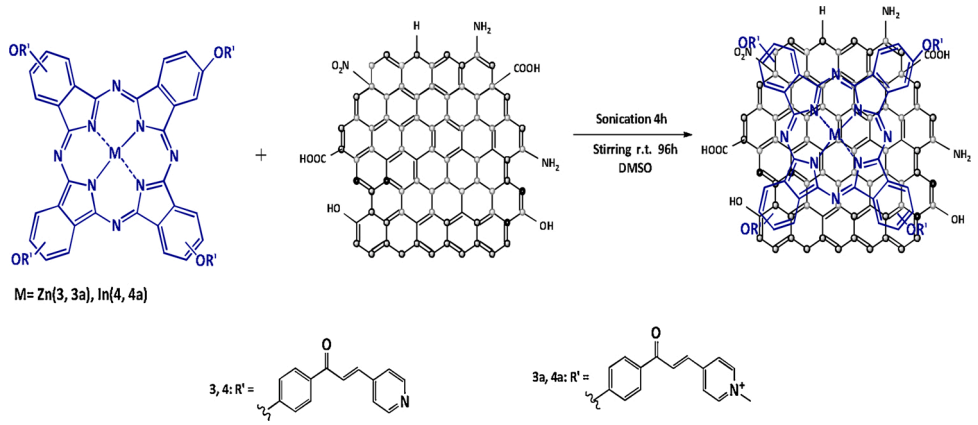

Scheme 2. MPcs@DNDs nanoconjugates synthesis.

mid logarithmic phase of growth was stopped once they reached an optical density (OD) value between 0.6−0.8 recorded at 620 nm. Afterward, the bacteria cultures were harvested by centrifugation (4000 RPM for 15 min) and then washed with phosphate buffer solution (PBS). The bacteria cultures were later diluted to 1/1000 in PBS to make working stock solutions of approximately 10^9 colony forming units (CFU) per mL for both type of bacteria. Photodynamic antimicrobial chemotherapy studies on *S. aureus* and *E. coli* were done following literature with slight changes [33,35] where, for comparison purposes, 1% DMSO in PBS solution was used as the solvent.

The concentration optimization of the Pcs was performed by using Pcs at different concentrations of 0.31, 0.63, 1.25, 2.5, 5, 10, 20 and 40 μg/mL. In all cases, firstly, solutions containing the photosensitizer and bacteria were incubated for 30 min in the dark at 37 °C. Afterward, 2.5 mL of the samples containing the photosensitizer and bacteria was irradiated for 30 min at the 670 nm in 24 well plate using a Modulight laser lamp (irradiance: 524 mV/cm and dose: 943 J/cm) while the other 2.5 mL was kept in the dark for 30 min to determine dark toxicity activity of the photosensitizers. For both the irradiated and non-irradiated samples, 100 μL of each sample was aseptically inoculated on nutrient agar plates in triplicates, followed by incubation for 18 h at 37 °C, at the end of which the colony counting was done. The control samples contained only bacteria and 1% DMSO in PBS without the drug [29].

For the time studies optimization, bacterial suspensions containing the optimized concentration of Pcs were prepared and the antimicrobial assays were done similarly as described above. In this case 2.5 mL of the suspension was kept in the dark and 2.5 mL was irradiated for 120 min at 30 min irradiation intervals starting from 0 min. Afterwards, the dark and irradiated treated suspensions were respectively inoculated on agar and the number of the formed colonies on each petri dish was counted after a period of 18 h incubation at 37 °C. A control experiment was also performed as stated above for both the dark and irradiation studies. The acquired CFU/mL data were then converted to the log reduction values and percentage cell survival.

2.3.2. Biofilm formation

The single-species biofilms of *S. aureus* and *E. coli* were prepared as following: Freshly prepared suspensions of each bacterial species at 10^6 CFU/mL were individually suspended in tryptic soy broth to obtain a concentration of 10^7 CFU/mL. From each newly prepared suspension, 200 μL was removed and seeded in 96 well plates then incubated statically and anaerobically at 37 °C for 5 days to allow the cell adhesion to the surface. Unbound planktonic cells were gently washed out using PBS and 200 μL of fresh tryptic soy broth was added daily to stimulate biofilm formation whose growth was monitored by microscope.

At the incubation completion, the biofilm-coated wells of the 96 well-plates were carefully washed twice with 200 μL of PBS and left to air dry for 30 min. To determine the formation of the biofilm, to each well of the plate, aqueous crystal violet solution (200 μL of 1%) was added and this was left to stain the biofilm for 30 min, then the optical density was determined at 570 nm. Subsequently, PBS was used to rinse the wells and remove the excess dye before air drying the plate [36,37].

In this experiment, the 96-well plates containing biofilms were inoculated with Pcs alone or nanoconjugates (100 μL) at different concentrations of 50 and 100 μg/mL in triplicates. And the wells where Pcs were not added, were considered as the control samples. After 30 min of incubation time in the dark at 37 °C, the biofilms were irradiated at 670 nm with the Modulight laser lamp (irradiance: 524 mV/cm and dose: 943 J/cm) for 2 h with 30 min time intervals. After irradiation, the suspensions were subjected to serial dilution using PBS, and 100 μL of each sample was aseptically inoculated on agar plates then incubated for 18 h at 37 °C to determine the number of colony-forming units per millilitre.

2.3.3. Statistical analysis

Three independent (n = 3) experiments were conducted in triplicates and the obtained data were compared using a 3-way factorial ANOVA. The data are presented as means ± standard deviation (SD). A *p*-value of 0.05 was considered statistically significant.

3. Results and discussion

3.1. Synthesis and characterization

The synthetic routes of compounds (**1**, **2**, **3**, **4, 3a** and **4a**) are shown in Scheme 1. In the first step, compound **1** was synthesized following Claisen-Schmidt condensation reaction of 4-hydroyacetophenone and 4-pyridinecarbaxaldehyde [38] and in the second step, the synthesised phthalonitrile **2** was obtained *via* base-catalyzed aromatic substitution reaction of **1** under argon atmosphere using K_2CO_3 as the base in dry DMF at 60 °C for 24 h [39]. Phthalocyanines **3** and **4** were prepared by cyclotetramerization reaction [40] of compound **2**, in DMAE (for **3**) or quinoline (for **4**) with few drops of DBU in the presence of anhydrous zinc acetate and indium chloride salts, respectively, under argon atmosphere. For the quaternized derivatives **3a** and **4a,** MPcs **3** and **4** were respectively reacted with excess CH_3I in DMF and acetone at room temperature to obtain positively charged and water soluble Pcs. The structures of the synthesized compounds were analysed by FT-IR, ^{1}H NMR, ^{13}C NMR, MS and UV–vis techniques (see Figs. S1–S10, in the Supporting Information, SI for NMR and mass spectra).

Compound **1** was obtained as yellow powder, with a protonated molecular ion peak $[M+H]^+$ at $m/z = 226.39$ in the MS spectrum corresponding to a molecular formula $C_{14}H_{11}NO_2$ (Fig. S1 in SI). ^{1}H NMR (Fig. S5) exhibited two doublet peaks at 8.12 and 7.61 corresponding to *trans* protons and a broad singlet peak at 10.58 corresponding to the OH proton while in ^{13}C NMR (Fig. S6) δ_C 142.3 and 126.8 corresponded to

the alpha, beta-unsaturated carbons and 187.3 (C═O). The ^{1}H and ^{13}C NMR data (Figs. S7 and S8) of compound **2** were in agreement with the proposed structure, exhibiting the disappearance of characteristic peaks such as —OH proton peak and the appearance of -CN carbon peaks at 115.5 in the ^{13}C NMR spectrum as shown in Fig. S8 in SI with *m/z* = 352.14 corresponding to $C_{22}H_{13}N_3O_2$ (Fig. S2 in SI).

The ^{1}H NMR spectra for MPcs **3**, **4**, **3a** and **4a** exhibited aromatic proton peaks ranging from 8.97 to 7.28 ppm (Figs. S9 and S10, using MPcs **4** and **4a** as examples). And the methyl protons were observed as singlets at around 2.90 ppm for the quaternized derivatives. In the acquired mass spectra of the Pcs, the expected molecular ion peaks were obtained at *m/z* = 1471.88 $[M+H]^+$ for **3**, *m/z* = 1555.26 $[M]^+$ for **4**, *m/z* = 1531.99 $[M+H]^+$ for **3a** and *m/z* = 1616.39 $[M+H]^+$ for **4a**. These results were in good agreement with the suggested structures (Figs. S3 and S4 using MPcs **3** and **4** as examples). The nanoconjugates of the synthesized Pcs and detonation nanodiamonds were acquired by π-π interactions between the two (Scheme 2).

3.1.1. UV–vis spectra

Fig. 1A illustrates the UV–vis spectra of the synthesized phthalocyanines in DMSO. The Q bands of all the Pcs exhibited monomeric behavior in DMSO. The spectra show intense absorption at 684 nm (for **3**), 686 nm (**4**), 683 nm (for **3a**) and 684 nm (for **4a**) (Table 1). InPc (**4**) showed a slight red spectral shift as compared to ZnPc (**3**), this is supported by the non-planar effect of the indium (III) ion, which as a relatively bigger atomic radius than the zinc (II) [41], resulting in the red shift in the former. There were insignificant shifts in the Q band maxima following quaternization, Table 1. Following conjugation of Pcs to DNDs, slight red shifts are observed (Fig. 1C), except for **4a**.

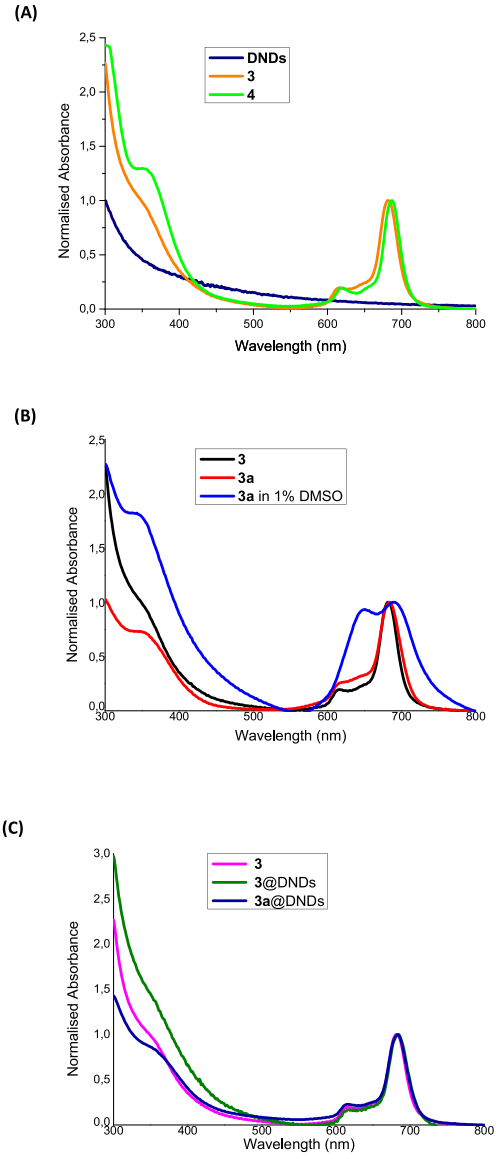

Fig. 1. Electronic absorption spectra of: (A) DNDs and phthalocyanines (**3** and **4**) in DMSO; (B) **3** in DMSO, and **3a** in 100 % DMSO and 1 % DMSO, and (C) **3**, **3**@DNDs and **3a**@DNDs in DMSO.

In 1% DMSO solution, aggregation was observed in the UV–vis absorption spectra of the quaternized derivatives as they exhibited two non-vibrational peaks in the Q band region [42], Fig. 1(B), Table 1. The red-shifted bands present at 688 (for **3a**); 688 (for **3a**@DNDs) nm and 691 nm (for **4a**); 690 nm (for **4a**@DNDs), respectively, are due to the monomeric species, whereas the blue-shifted bands at 650 (for **3a**); 651 (for **3a**@DNDs) nm and 651 (for **4a**); 651 (for **4a**@DNDs) nm are due to the aggregation.

Following π-π interactions formed between the Pcs and DNDs π systems (Scheme 2), an enhancement in absorption below 600 nm, Fig. 1 (C), due to absorption by DNDs.

Loading of Pcs unto DNDs was done spectroscopically *via* UV–vis spectra as previously reported [43,44], where the quaternized Pcs@DNDs had a greater mass loading of 737 and 536 μg (Pc)/mg (DNDs) for **3a**@DNDs and **4a**@DNDs respectively, as compared to the non-quaternized counterparts with mass loading of 383 and 146 μg (Pc)/mg (DNDs) for **3**@DNDs and **4**@DNDs respectively, Table 1. This could be justified by the electrostatic interactions between the positive charges on the Pcs and the negative charges created by π electrons on the DNDs sheets for **3a**@DNDs and **4a**@DNDs, hence larger loading. And the smaller Pc mass loadings observed in the indium derivatives is due to the presence of chlorine axial ligand on the InPc that may limit the number of Pcs loaded due to the bulkiness [45].

3.1.2. FT-IR spectra

The data from FT-IR also confirmed the suggested structures. The C≡N vibration for **2** at 2231 cm^{-1}, disappeared following cyclotetramerization reaction to form the MPcs, Fig. 2. This is indicating the successful formation of targeted molecules.

Peaks appearing at 3056−3055 cm^{-1} and 2923−2855 cm^{-1} are attributed to stretching vibrations of aromatic C—H and aliphatic C—H bonds, respectively. The peaks at 1583−1491 cm^{-1} are due to C═C and C═N vibrations, while peaks appearing around 1722−1721 cm^{-1} are associated to the C═O groups for the Pcs alone. In the FT-IR spectra of the Pcs@DNDs nanoconjugates, the C═O peaks showed high intensities as compared to the Pcs counterparts, this can be explained by the larger number of C═O groups in the conjugates which are from both the Pcs and the DNDs. Broader vibration peaks with higher intensities at 3056 cm^{-1} in the spectra of the nanoconjugates spectra are associated to the OH and NH_2 stretching from DNDs, confirming the successful conjugation to MPcs. Shifts in FT-IR spectra are an indication that molecular interactions have taken place.

3.1.3. Raman spectra

In the current study, Raman spectroscopy was conducted to determine the quality of the DNDs and that of the prepared π-π stacked nanoconjugates. The G-band (sp^2) tangential mode was observed at 1593 cm^{-1} and the D-disorder band (breathing mode, sp^3) was observed at 1371 cm^{-1} (Fig. 3) [46,47] for DNDs alone. In the spectra of the conjugates, the G bands shifted to higher frequencies of 1597 and 1595 cm^{-1} for **3**@DNDs and **4**@DNDS respectively, while the G bands shifted to lower frequencies of 1568 and 1574 cm^{-1} for **3a**@DNDs and **4a**@DNDs, respectively. On the other hand, the D bands shifted to higher frequencies of 1379 and 1389 cm^{-1} for **3a**@DNDs and **4a**@DNDs, respectively. There were no shifts in the D-bands of the neutral Pcs@DNDs (Fig. 3 using **4**@DNDNs as an example). The larger

Table 1
Photophysicochemical parameters of the DNDs, Pcs alone and different nanoconjugates in DMSO.

Sample[a]	Abs.[b]	Em.	Loading (μg Pc/mg DNDs)	Raman I_D/I_G	Φ_F	τ_F (ηs)	Φ_Δ
DNDs (2.4 nm)	–	–		0.26	–	–	–
3	684	695	–	–	0.072	2.97	0.39
3a	683 (688, 650)	693	–	–	0.067	2.84	0.43 (0.21)[b]
4	686	693	–	–	0.043	2.91	0.50
4a	684 (691, 651)	689	–	–	0.020	2.26	0.53 (0.27)[b]
3@DNDs (8 nm)	687	694	383	0.34	0.045	2.81	0.51
3a@DNDs (13 nm)	690 (688, 651)	693	737	0.59	0.031	2.22	0.61 (0.46)[b]
4@DNDs (18 nm)	689	691	146	0.34	0.036	2.49	0.68
4a@DNDs (22 nm)	684 (690, 651)	689	536	0.59	0.020	2.02	0.69 (0.47)[b]

[a]Values in brackets are TEM sizes.
[b]Values in brackets are in water which is used for cell studies.

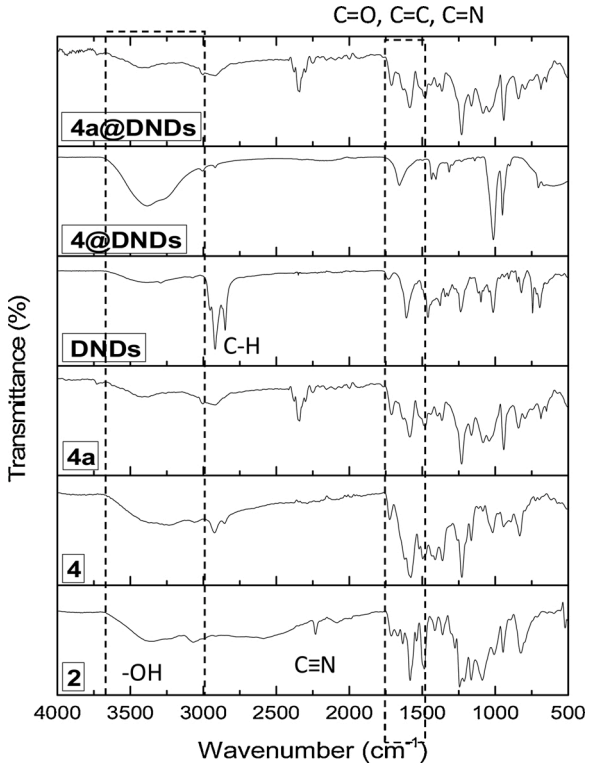

Fig. 2. FT-IR spectra of **2**, **4**, **4a**, DNDs, **4**@DNDs and **4a**@DNDs.

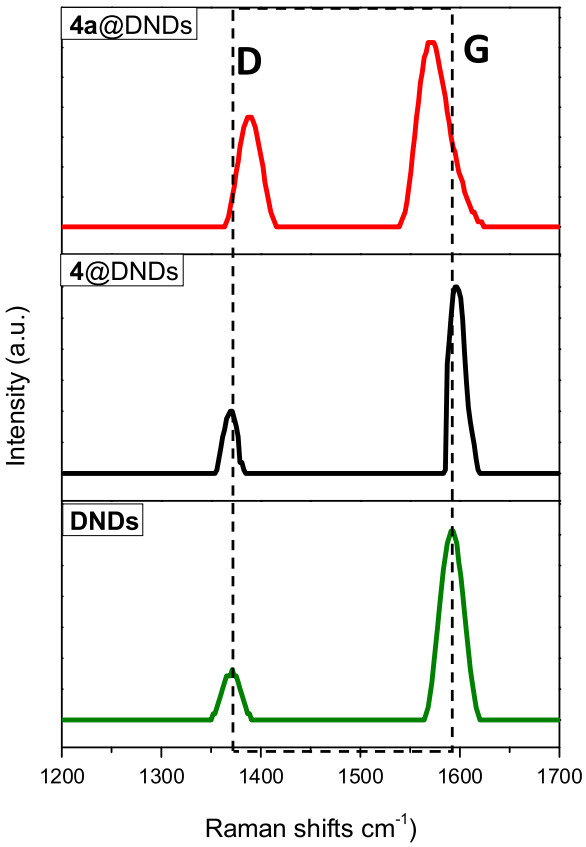

Fig. 3. Raman spectra of DNDs alone, **4**@DNDs and **4a**@DNDs (as example s).

shifts and increase in the intensities of D-bands in the positively charged nanoconjugates may be due to more interaction from both π–π and electrostatic interactions. As literature states, shifts in the Raman frequencies are always an indication of strong π electron interactions between the Pcs and carbon nanomaterial such as DNDs [48].

The ratio of the intensities of the D and G bands (I_D/I_G) can provide information on the quality of extent of functionalization in the DNDs. The I_D/I_G obtained value was 0.26 for DNDs alone, while I_D/I_G values were about 0.34 for neutral Pcs@DNDs (**3**, and **4**) and 0.59 for the positively Pcs@DNDs (**3a** and **4a**), Table 1. The increase in the I_D/I_G value observed implies that there is presence of sp^3 defects from Pcs on the sp^2 lattice of the DNDs which enhances the D-band [49].

3.1.4. Transmission Electron Microscopy (TEM)

To determine the morphology and size of the prepared DNDs and Pcs@DNDs nanoconjugates, we made use of the TEM technique (Figs. 4 and S11 in SI). The obtained images confirmed that the DNDs were spherical and monodispersed. Fig. 4 gave the DNDs size of 2.4 nm. However, on conjugation, an increase on the sizes of Pcs@DNDs conjugates is observed as the sizes increased to ~ 8, 13, 18 and 22 nm for **3**@DNDs and **3a**@DNDs, **4**@DNDs and **4a**@DNDs respectively, Table 1. The increase in size is due to aggregation following conjugation of Pcs to nanoparticles.

3.2. Photophysicochemical properties

3.2.1. Emission, Fluorescence quantum yield (Φ_F) and Fluorescence lifetime (τ_F)

The emission spectra were recorded in DMSO and were mirror images of the excitation spectra which are found to be similar to the absorption spectra proving that the molecules that are emitting light are the same as those that are absorbing light (Fig. 5). The measurements of the emission wavelengths are reported in Table 1. Slight the shifts between excitation and absorption spectra in Fig. 5, may be due to different equipment used.

The obtained Φ_F values are low (equations in Supporting Information) at 0.072, 0.067, 0.043, 0.020, 0.045, 0.031, 0.036 and 0,020 for **3**,

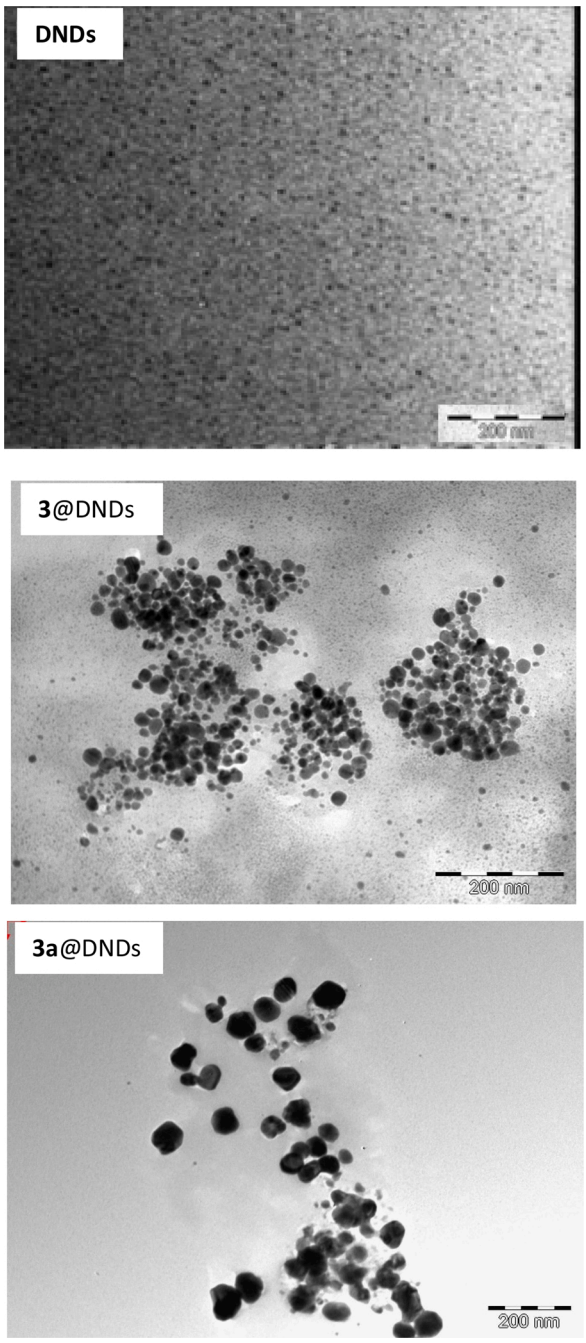

Fig. 4. TEM images of DNDs, **3**@DNDs and **3a**@DNDs nano-assemblies (as examples) showing the morphology and size increase upon conjugation.

3a, **4**, **4a**, **3**@DNs, **3a**@DNDs, **4**@DNDs and **4a**@DNDs in DMSO, respectively. These low values (lower than the standard ZnPc at 0.20 in DMSO [31]) could be to the quenching effect the substituent. The type of substituent on the Pc macrocycle is known to affect Φ_F values [50]. The Φ_F values of InPcs are lower than those of ZnPc counterparts since In (III) is a heavier metal than Zn (II). Heavy central metals are known to enhance the intersystem-crossing to the triplet state, thus reducing fluorescence [51].

The Φ_F values for the quaternized Pcs measured in PBS (1% DMSO) were not calculated due to their non-fluorescence behavior in this media. The Φ_F values of the quaternized Pcs were lower when compared to the non-quaternized entities. This may be explained by the fact that chalcone compounds are fluorescent, and their quaternization can inhibit fluorescence. The decrease in Φ_F values in the presence of DNDs,

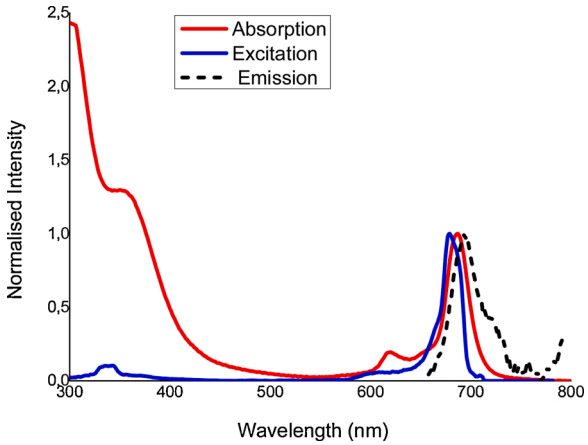

Fig. 5. Example of normalized absorption, excitation and emission spectra of **4** in DMSO, excitation 614 nm.

Table 1, could be due to the fact that electron donating groups are known to increase intersystem crossing in porphyrin-type complexes [52], reducing fluorescence. However the decrease is not observed for **4a**@DNDs compared to **4a**, Table 1, both with Φ_F value of 0.02.

Fluorescence lifetime (τ_F) is the average time a molecule remains in its excited state before returning to its ground state by emitting light [53]. The τ_F of the newly synthesized Pcs and nanoconjugates were obtained using the time correlation single photon counting (TCSPC) method (Fig. 6 using **4**@DNDs as an example). Mono-exponential decay curves were observed in all cases. The τ_F values were 2.97 ns (**3**), 2.84 ns (**3a**), 2.91 ns (**4**), 2.26 ns (**4a**), 2.81 ns (**3**@DNDs), 2.22 ns (**3a**@DNDs), 2.49 ns (**4**@DNDs), and 2.02 ns (**4a**@DNDs). The decreases in τ_F in the presence of DNDs corresponds to the decrease in Φ_F values, the two change in unison.

3.2.2. *Singlet oxygen quantum yield (Φ_Δ)*

Similar to PDT, PACT process also relies on singlet oxygen ($^1O_2$) generated at the end of the energy transfer between the triplet state of a photosensitizer and ground state molecular oxygen [54]. Singlet oxygen quantum yield (Φ_Δ) is a significant parameter used to quantify the efficiency of a photosensitizer to produce $^1O_2$. In the current study, the determination of Φ_Δ values was done by the means of a chemical method using 1,3-diphenylisobenzofuran (DPBF) and 9,10-antracenediyl-bis (methylene)dimalonoic acid (ADMA) as singlet oxygen quenchers in DMSO and aqueous media, respectively. We monitored the decrease in absorbance of DPBF at 417 nm and ADMA at 380 nm using UV–vis spectrophotometer (Fig. 7A and B, **4a** was used as an example). Fig. 7A

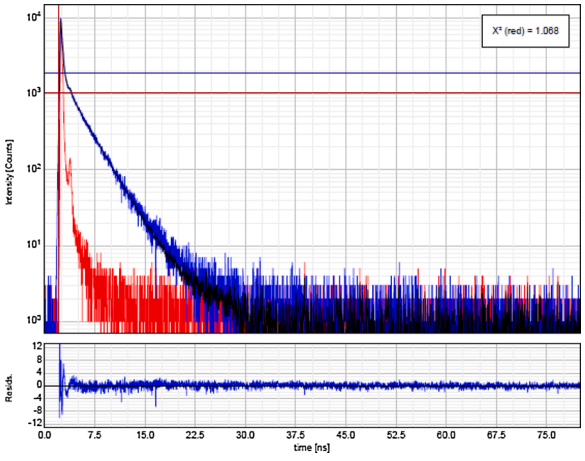

Fig. 6. TCSPC fluorescence decay curve of **4**@DNDs (as an example).

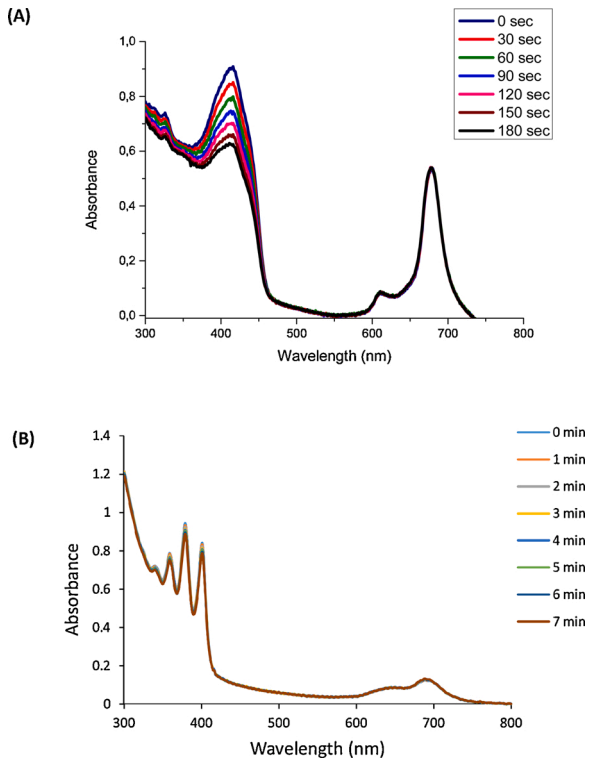

Fig. 7. A typical spectrum for the determination of singlet oxygen quantum yield of (A) **4a** in DMSO using DPBF and (B) **4a** in 1%DMSO using ADMA.

and B indicate no significant change in the absorption intensities of the Q-band of the phthalocyanines, this suggests that the Pcs are stable during irradiation. Similar trends were observed for the nanoconjugates as well. The Φ_Δ values were determined in DMSO for the studied phthalocyanines, and 1% DMSO (in PBS) (Table 1). The Φ_Δ data are given in Table 1. The Φ_Δ values in Table 1 range between 0.39 and 0.69 in DMSO with the indium derivatives showing the highest values. The higher Φ_Δ values of 0.51, 0.61, 0.68 and 0.69 obtained for **3**@DNDs, **3a**@DNDs, **4**@DNDs and **4a**@DNDs nanoconjugates, respectively, in DMSO compared to MPcs alone is due to the increased intersystem crossing in the presence of DNDs discussed above. Φ_Δ values are higher for the InPc derivatives (**4** and **4a** and their conjugates) compared to corresponding ZnPc derivatives (**3** and **3a** and their conjugates) due to the heavy atom effect of In. The Φ_Δ values obtained for the quaternized derivatives were higher compared to the non quaternized counterparts in DMSO. This may be due to the absence of photoinduced electron transfer (PET) process between phthalocyanine macrocycle and the substituents since the lone pair electrons of nitrogen atoms are bonded to methyl groups [54].

Previous reports state that the presence of nitrogen atoms in graphitic materials generates charged sites that augment the adsorption of oxygen [55]. This may also result in the observed enhanced Φ_Δ in the presence of DNDs. Values in water (1 % DMSO), Table 1, are low due to quenching of singlet oxygen by water [31]. The new synthesized chalcone substituted Pcs and conjugates have sufficient singlet oxygen capability as photosensitizers for PACT applications.

3.3. PACT studies

PACT activities against *S. aureus* and *E. coli* were evaluated using the newly prepared photosensitisers. The principle of PACT is based on phototoxic and chemical reactions, which cause death of bacterial free cells or biofilms following irradiation of a photosensitizer by a light in the presence of molecular oxygen [56,57]. For the efficiency of PACT process, the photosensitizer should be able to efficiently bind to the cell-wall, this will facilitate its penetration and ability to act within the cell since the generation of singlet oxygen is done within the cell [58]. Hence, in the current work, we developed positively charged photosensitizers that have efficient inactivation of gram-positive but especially gram-negative bacteria for strong photo-antibacterial effectiveness.

The optimal concentrations, which are the lowest concentrations at which compounds can still exhibit antimicrobial potency by inhibiting more than 50 % of the bacteria, were found to be at 10 μg/mL and 1.25 μg/mL for the non-quaternized and quaternized Pcs (and their conjugates), respectively on planktonic cells.

For the *E. coli* and *S. aureus* biofilms studies, a concentration of 100 μg/mL of each of the synthesized compounds were used to determine the photo-antibiofilm activity after 30 min of irradiation at 670 nm.

3.3.1. *In vitro antibacterial activity on planktonic cells*

Each of the non-quaternized compounds (10 μg/mL) or quaternized compounds (1.25 μg/mL) and their conjugates were dissolved in 1% DMSO in PBS solutions. The control solutions were made up of 1% DMSO in PBS without the photosensitizers. The controls showed no antibacterial effect on the studied bacteria, Fig. 8A, B, C and 9A, B, C.

The samples were also subjected to dark toxicity studies which confirmed that the photosensitizers possessed no dark toxicity, as the results displayed no significant change in log (CFU, colony forming units) in Figs. 8A and 9 A for studies conducted on *S. aureus* and *E. coli*, respectively.

For the photoinhibition studies, samples containing the synthesized compounds and bacteria were irradiated at 670 nm using a Modulight laser. As displayed in Figs. 8B, 9 B and Table 2, quaternized Pcs and their Pcs@DNDs counterparts were able to effectively kill both different bacteria strains at lower concentrations and in a short period of time. The efficient killing of bacteria strains by the positively charged compounds is expected as the compounds are not only water soluble but also present stronger affinity to the cell-wall thus resulting in complete cell membrane destruction and enhanced drug-cell uptake for efficient photo-antibacterial abilities since they are producing the singlet oxygen in a close proximity of the cell.

For *S. aureus*, a log reduction of 9.60 ± 0.002 for **3a** and **4a** after 30 min and the same value of 9.60 ± 0.001 for **3a**@DNDs and **4a**@DNDs but at a higher irradiation time of 60 min were obtained for *S. aureus* showing no advantage of DNDs, Table 2. The log reductions for non-quaternized **3**, **4** and **3**@DNDs were lower compared to corresponding quaternized derivatives even at a high irradiation time of 120 min, thus showing the importance of the positive charges as a result of quaternization, Table 2. **4**@DNDs (even though containing an unquaternized Pc) had a high log reduction value (9.27 ± 0.003) most likely due to the high singlet oxygen quantum yield which is almost the same as for **4a**@DNDs, Table 1. Comparing **3** and **4** and their conjugates shows improvement in terms of log reductions in the presence of DNDs, even though that was not the case for quaternized derivatives.

For *E. coli*, **3a** and **4a** gave log reductions values of 9.64 ± 0.002 after 30 min irradiation. These values increased in the presence of DNDs (for **3a**@DNDs and **4a**@DNDs, respectively) corresponding to the increase in singlet oxygen quantum yield, Table 2.

The non quaternized Pcs alone had less activities against both strains, with compound **3** exhibiting 0.52 ± 0.001 $\log_{10}$ CFU reduction (28.98 % cell survival) and 0.15 ± 0.003 $\log_{10}$ CFU reduction (57.16 % cell survival) when treating *S. aureus* and *E. coli*, respectively. On the other hand, **4** presented a 1.85 ± 0.002 $\log_{10}$ CFU reduction (1.54 % cell survival) and 0.48 ± 0.001 $\log_{10}$ CFU reduction (27.2 % cell survival) when treating *S. aureus* and *E. coli* respectively, whereas, the DNDs alone showed no major activity in both cases.

The lower activities observed for the non quaternized compounds against *E. coli* as compared to *S. aureus* is expected as literature reports the double-layered cell membrane of gram-negative bacteria being a

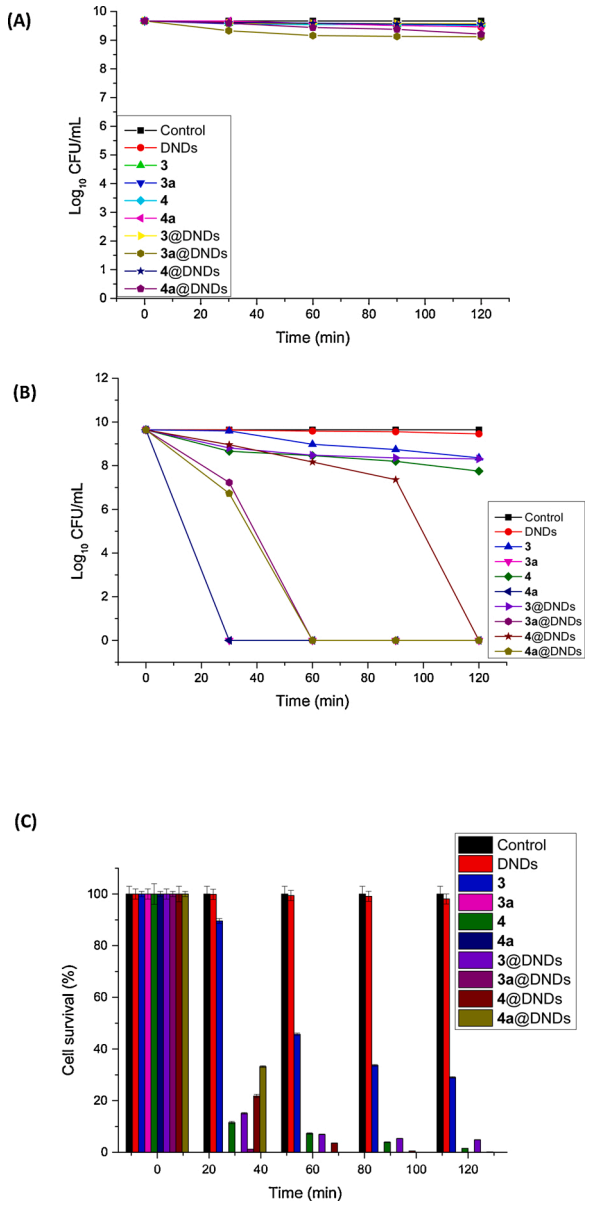

Fig. 8. Log CFU plots for (**A**) Dark toxicity studies and, (**B**) photoinhibition, and (**C**) cell survival for *S. aureus* planktonic cells in the presence of Pcs alone and the Pcs@DNDs conjugates (irradiation at 670 nm). Concentration of the Pcs and conjugates =10 μg/mL for non quaternized and 1.25 μg/mL for the quaternized. Data represent the mean ± SD.

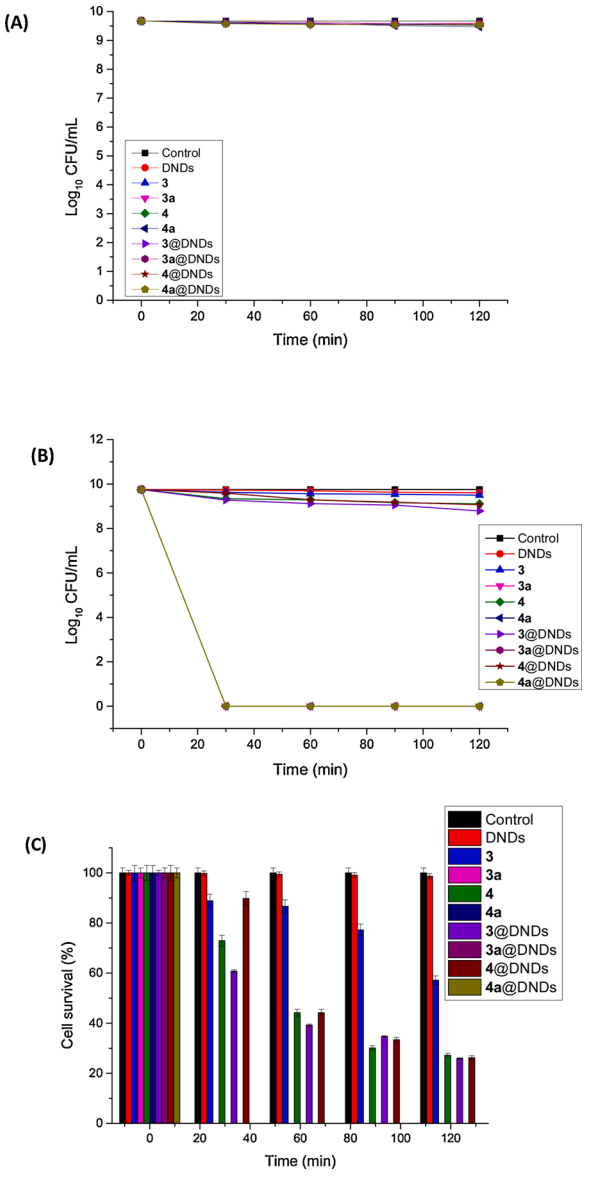

Fig. 9. (**A**) Dark toxicity studies, (**B**) photoinhibition and (**C**) cell survival for *E. coli* planktonic cells in the presence of Pcs alone and the Pcs@DNDs conjugates (irradiation at 670 nm). Concentration of the Pcs and conjugates 10 μg/mL for non quaternized and 1.25 μg/mL for the quaternized. Data represent the mean ± SD.

barrier to neutral photosensitizers access inside the cell. Since PACT process relies on singlet oxygen production by the photosensitizer, the resulting data of this work are in perfect agreement with singlet oxygen quantum yields values obtained and also this confirms the importance of conjugation of photosensitizers to carbon nanomaterials that have also been reported to possess intrinsic antibacterial properties. The synthesized nanoconjugates showed better PACT activities corresponding to high singlet oxygen quantum yields.

3.3.2. *In vitro biofilms eradication*

Different concentrations 50 and 100 μg/mL of photosensitizers were used for biofilms photoinhibition studies. The treatment doses were increased in this case due to the non-sensitivity of biofilms toward antimicrobial treatment compared to the planktonic cells. This is mainly caused by the composition of the extracellular polymeric matrixes of biofilms that prevents in most cases the penetration of the drugs and therefore this favors the failure of many known treatments [59,60].

The quantification of biofilms formation by crystal violet assays showed that *S. aureus* and *E. coli* strains are strong biofilm producers under the used working conditions. In Figs. 10A and 11 A, it is illustrated that all the compounds did not show antibiofilm activity at 50 μg/mL but some activity was observed while using 100 μg/mL of each compound. For this reason, the time studies to determine the therapeutic efficacy of the new photosensitizers were carried on using the concentration of 100 μg/mL in all cases.

For *S. aureus* biofilms, **3a**@DNDs and **4a**@DNDs showed highest value of 9.68 $\log_{10}$ CFU reduction with total photoinhibition of biofilm cells, while **3a** and **4a** respectively gave values of 1.40 $\log_{10}$ CFU reduction (cell survival of only 5.85 %) and 2.13 $\log_{10}$ CFU reduction (cell survival of only 0.36 %), all after 120 min of irradiation (Fig. 10B, Table 3). While **3**@DNDs and **4**@DNDs presented log CFU reductions of 0.3 and 1.63 respectively.

As displayed in Fig. 11B, only the indium derivatives **4a** and

Table 2
Log reduction and Cell survival (%) values of 10 μg/mL for non quaternized and 1.25 μg/mL for quaternized samples in 1% DMSO/PBS after irradiation.

Samples	*S. aureus*			*E. coli*		
	Log reduction	Cell Survival (%)	Time of irradiation (min)	Log reduction	Cell Survival (%)	Time of irradiation (min)
3	0.52±0.001	28.98	120	0.15±0.003	57.16	120
3a	9.60±0.002	0	30	9.64±0.002	0	30
3@DNDs	1.32±0.004	4.81	120	0.74±0.003	25.92	120
3a@DNDs	9.60±0.001	0.15	60	9.64±0.003	0	30
4	1.85±0.002	1.54	120	0.48±0.001	27.2	120
4a	9.60±0.001	0	30	9.64±0.002	0	30
4@DNDs	9.27±0.003	0.17	120	0.58±0.003	26.23	120
4a@DNDs	9.60±0.001	0	60	9.64±0.002	0	30

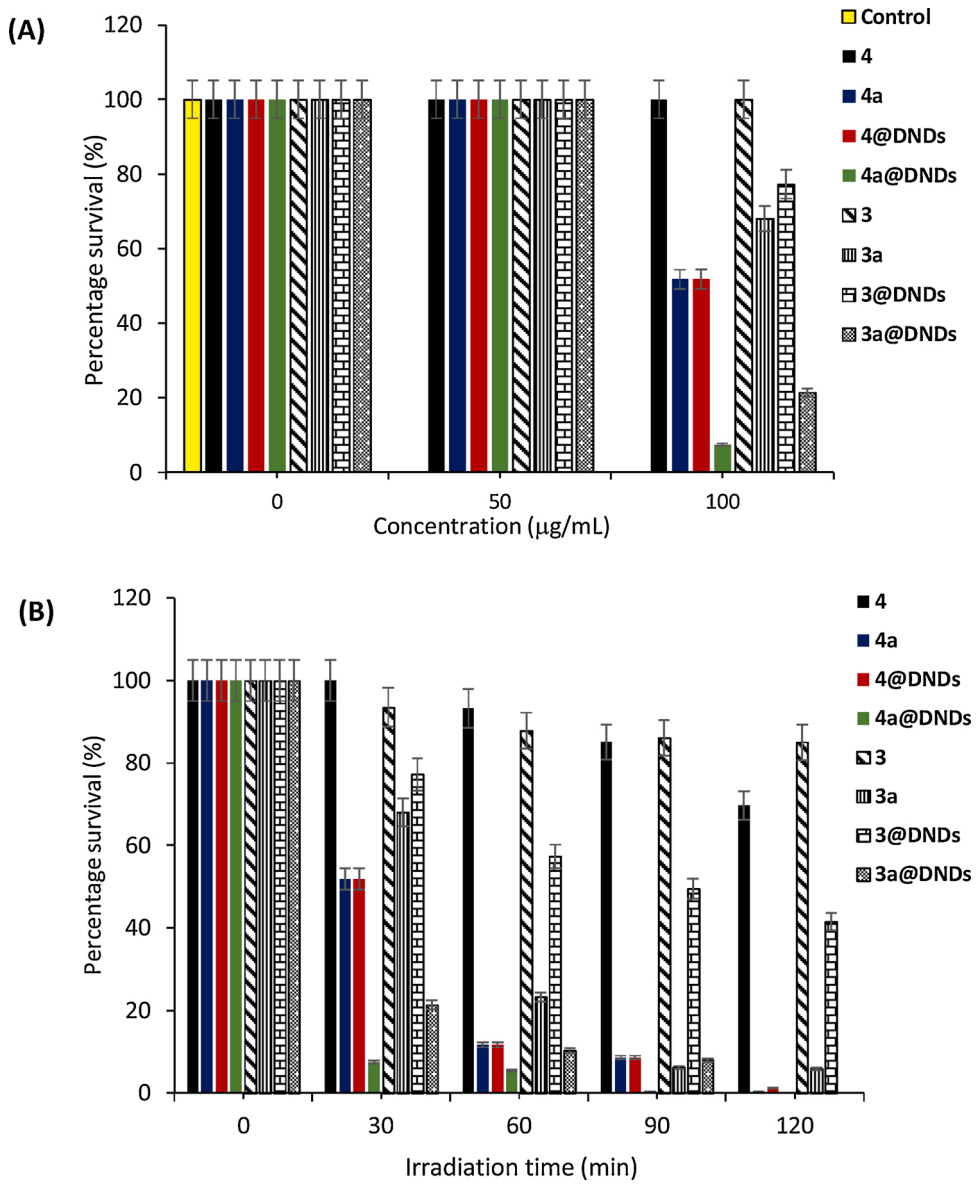

Fig. 10. Survival graph of photodynamic antimicrobial chemotherapy on *S. aureus* biofilm (**A**) after 30 min of irradiation at concentration of 50 and 100 μg/mL and (**B**) variation of cell survival for all the synthesized at 100 μg/mL with time up to 120 min irradiation. Data represent the mean ± SD.

4a@DNDs were able to totally kill *E. coli* cells in biofilm at 100 μg/mL upon 120 min of irradiation, with 9.80 $\log_{10}$ CFU reduction with no cell survival for both compounds. And statistical significant reductions in biofilm with 1.45, 1.43, 1.38 and 2.24 $\log_{10}$ CFU were obtained in viable count for **3a**, **3**@DNDs, **3a**@DNDs and **4**@DNDs, respectively.

Non quaternized Pcs alone **3** and **4** showed no major reductions in biofilms in comparison to the respective untreated control groups for all the strains. The great decrease in biofilms cell viability and the complete eradication of the two singled biofilm species under light conditions observed in the quaternized nanoconjugates could be due to the

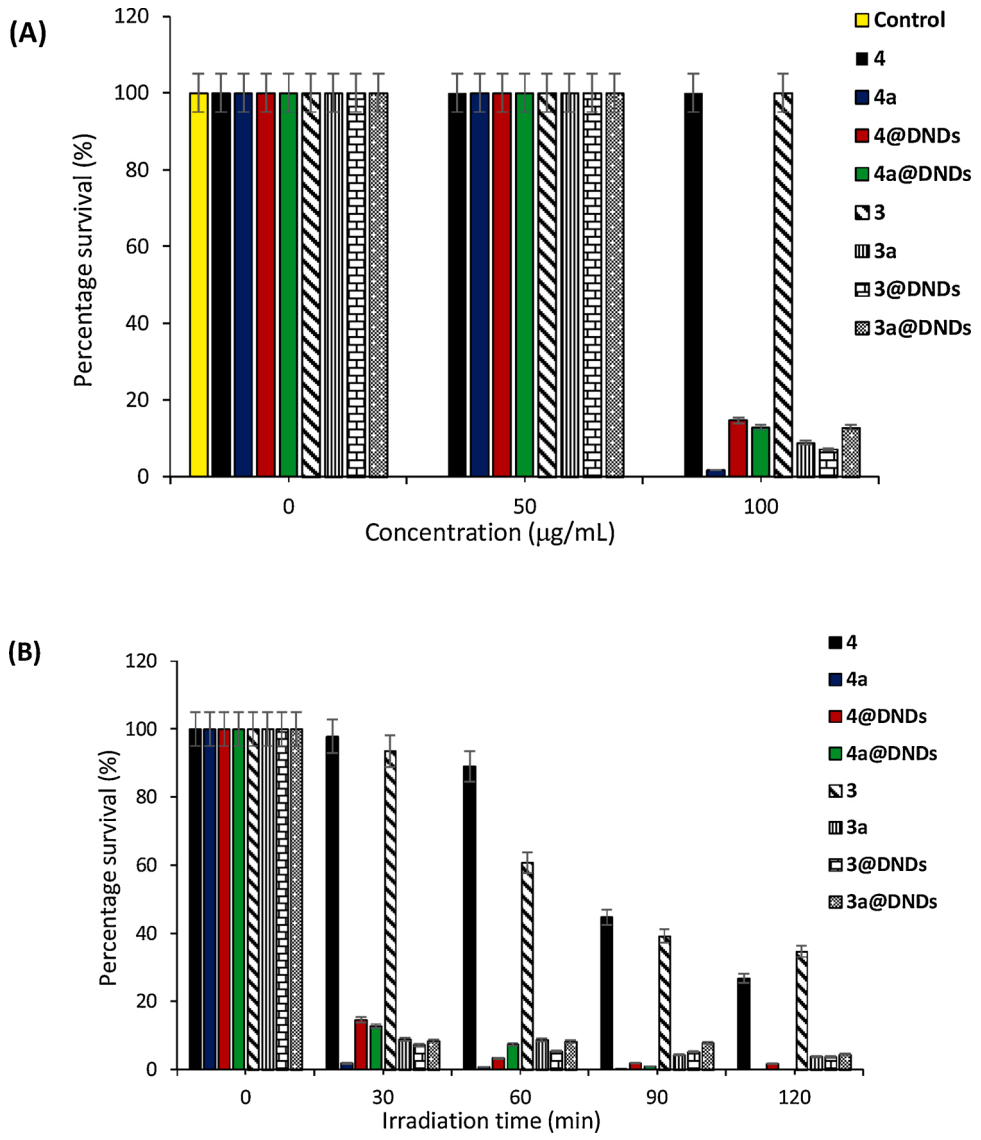

Fig. 11. Survival graph of photodynamic antimicrobial chemotherapy on *E. coli* biofilm (**A**) after 30 min of irradiation at concentration of 50 and 100 µg/mL and (**B**) variation of cell survival for all the synthesized at 100 µg/mL with time up to 120 min irradiation. Data represent the mean ± SD.

Table 3
Log reduction values for biofilms at 120 min.

MPcs/conjugate	*S. Aureus*	*E. Coli*
3	0.07	0.33
3a	1.40	1.45
3@DNDs	0.3	1.43
3a@DNDs	9.68	1.38
4	0.15	0.58
4a	2.13	9.80
4@DNDs	1.63	2.24
4a@DNDs	9.68	9.80

synergistic effect brought by the DNDs and the Pc alone, the positive charges and the high singlet oxygen quantum yields.

The basic mode of action of the new compounds studied might include inhibition of cell metabolism and growth, damage to the cytoplasmic membrane and increase in cell permeability due the charges found on the moieties [61,62]. All of the obtained data further confirm that the newly prepared nano photosensitisers could be used as potential photoantibacterial agents against *Staphylococcus aureus* and *Escherichia coli* planktonic cells and biofilms at low concentrations of the complexes with small light doses.

4. Conclusion

Novel quaternized and non-quaternized zinc and indium chalcone substituted phthalocyanines and their corresponding π-π interactions to DNDs nanoconjugates are reported for the first time. The prepared compounds showed the ability to produce singlet oxygen and have high potential in the eradication of not only the bacterial planktonic cells of *S. aureus* and *E. coli*, but they also possessed great activities against their difficultly treated bacterial biofilms. This study also reports on the characterization and photophysicochemical parameters of all the synthesized compounds. The indium derivatives and the Pcs@DNDs showed in most cases, high singlet oxygen quantum yields, mainly with the quaternized compounds. The photo-antimicrobial activities of all the complexes/conjugates using PACT with irradiation at 670 nm were determined for all the compounds. It was revealed that the quaternized nanoconjugates had the highest activity against planktonic cells of *S. Aureus* and *E. coli,* with the highest log reductions causing total deaths of the planktonic cells and cells in the biofilms. The *in vitro* results indicate that at lower concentration the synthesized photosensitisers

have a great prospective in biofilms ablation.

CRediT authorship contribution statement

Yolande Ikala Openda: Conceptualization, Investigation, Writing - original draft. **Tebello Nyokong:** Supervision, Resources, Writing - review & editing, Funding acquisition.

Declaration of Competing Interest

The authors report no declarations of interest.

Acknowledgements

This work was supported by the Department of Science and Innovation (DSTI) and National Research Foundation (NRF), South Africa through DSI/NRF South African Research Chairs Initiative for Professor of Medicinal Chemistry and Nanotechnology (UID 62620), Rhodes University, the Organization for Women in Science for the Developing World (OWSD) and Swedish International Development Cooperation Agency (Sida).

Appendix A. Supplementary data

Supplementary material related to this article can be found, in the online version, at doi:https://doi.org/10.1016/j.jphotochem.2021.113200.

References

[1] D. Hu, Y. Deng, F. Jia, Q. Jin, Jian Ji, Surface charge switchable supramolecular nanocarriers for nitric oxide synergistic photodynamic eradication of biofilms, ACS Nano 14 (2020) 347–359.
[2] L.C. Gomes, F.J. Mergulhão, SEM Analysis of surface impact on biofilm antibiotic treatment, Hindawi Scanning 2017 (2017), 2960194, https://doi.org/10.1155/2017/2960194.
[3] C.S. Vinagreiro, A. Zangirolami, F.A. Schaberle, S.C.C. Nunes, K.C. Blanco, N. M. Inada, G.J. da Silva, A.A.C.C. Pais, V.S. Bagnato, L.G. Arnaut, M.M. Pereira, Antibacterial photodynamic inactivation of antibiotic-resistant bacteria and biofilms with nanomolar photosensitizer concentrations, ACS Infect. Dis. 6 (2020) 1517–1526, https://doi.org/10.1021/acsinfecdis.9b00379.
[4] W. Wang, X. Cheng, J. Liao, Z. Lin, L. Chen, D. Liu, T. Zhang, L. Li, Y. Lu, H. Xia, Synergistic photothermal and photodynamic therapy for effective implant-related bacterial infection elimination and biofilm disruption using Cu9S8 nanoparticles, ACS Biomater. Sci. Eng. 5 (2019) 6243–6253.
[5] S. Szunerits, A. Barras, R. BoukherroubInt, Antibacterial applications of nanodiamonds, J. Environ. Res. Public Health 13 (2016) 413, https://doi.org/10.3390/ijerph13040413.
[6] M. Mirzahosseinipour, K. Khorsandi, R. Hosseinzadeh, M. Ghazaeian, F.K. Shahidi, Antimicrobial photodynamic and wound healing activity of curcumin encapsulated in silica nanoparticles, Photodiagn. Photodyn. Ther. 29 (2020), 101639.
[7] A. Taraszkiewicz, G. Fila, M. Grinholc, J. Nakonieczna, Innovative strategies to overcome bioflm resistance, BioMed. Research Internat. 2013 (2013), 150653, https://doi.org/10.1155/2013/150653.
[8] R. Tang, L.M. Habimana-Griffin, D.D. Lane, C. Egbulefu, S. Achilefu, Nanophotosensitive drugs for light-based cancer therapy: what does the future hold? Nanomedicine (Lond) 12 (2017) 1101–1105.
[9] A. Sindelo, O.L. Osifeko, T. Nyokong, Synthesis, photophysicochemical and photodynamic antimicrobial chemotherapy studies of indium pyridyl phthalocyanines: charge versus bridging atom, Inorg. Chim. Acta 476 (2018) 68–76.
[10] S. Afrasiabi, M. Pourhajibagher, N. Chiniforush, M. Aminian, A. Bahador, Anti-biofilm and anti-metabolic effects of antimicrobial photodynamic therapy using chlorophyllin-phycocyanin mixture against Streptococcus mutans in experimental biofilm caries model on enamel slabs, Photodiagn. Photodyn. Ther. 29 (2020), 101620.
[11] Y. Liu, R. Qin, S.A.J. Zaat, E. Breukink, M. Heger, Antibacterial photodynamic therapy: overview of a promising approach to fight antibiotic-resistant bacterial infections, J. Clin. Transl. Res. 1 (2015) 140–167.
[12] M.R. Hamblin, T. Hasan, Photodynamic therapy: a new antimicrobial approach to infectious disease? Photochem. Photobiol. Sci. 3 (2004) 436–450.
[13] T.J. Beveridge, Structures of gram-negative cell walls and their derived membrane vesicles, J. Bacteriol. 181 (1999) 4725–4733.
[14] F. Cieplik, L. Tabenski, W. Buchalla, T. Maisch, Antimicrobial photodynamic therapy for inactivation of biofilms formed by oral key pathogens, Frontiers Microbiol. 9 (2018) 405, https://doi.org/10.3389/fmicb.2014.00405.
[15] Z. Biyiklioglu, I. Ozturk, T. Arslan, A. Tunçel, K. Ocakoglu, M. Hosgor-Limoncu, F. Yurt, Synthesis and antimicrobial photodynamic activities of axially {4-[(1E)-3-oxo-3-(2-thienyl)prop-1-en-1-yl]phenoxy} groups substituted silicon phthalocyanine, subphthalocyanine on Gram-positive and Gram-negative bacteria, Dyes Pigm. 166 (2019) 149–158.
[16] M.P. de Filippis, D. Dei, L. Fantetti, G. Roncucci, Synthesis of a new water-soluble octa-cationic phthalocyanine derivative for PDT, Tetrahedron Lett. 41 (2000) 9143–9147.
[17] S.R. Wood, J.A. Holroyd, S.B. Brown, The subcellular localization of Zn (II) phthalocyanines and their redistribution on exposure to light, Photochem. Photobiol. 65 (1997) 397–402.
[18] F. Cieplik, L. Tabenski, W. Buchalla, T. Maisch, Antimicrobial photodynamic therapy for inactivation of biofilms formed by oral key pathogens, Front. Microbiol. 5 (2014) 1–17, https://doi.org/10.3389/fmicb.2014.00405.
[19] Y. Gao, B. Mai, A. Wang, M. Li, X. Wang, K. Zhang, Q. Liu, S. Wei, P. Wang, Antimicrobial properties of a new type of photosensitizer derived from phthalocyanine against planktonic and biofilm forms of Staphylococcus aureus, Photodiagn. Photodyn. Ther. 21 (2018) 316–326, https://doi.org/10.1016/j.pdpdt.2018.01.003.
[20] V. Mantareva, V. Kussovski, I. Angelov, D. Wöhrle, R. Dimitrov, E. Popova, S. Dimitrov, Non-aggregated Ga(III)-phthalocyanines in the photodynamic inactivation of planktonic and biofilm cultures of pathogenic microorganisms, Photochem. Photobiol. Sci. 10 (2011) 91–102, https://doi.org/10.1039/b9pp00154a.
[21] M.G. Strakhovskaya, Y.N. Antonenko, A.A. Pashkovskaya, E.A. Kotova, V. Kireev, V.G. Zhukhovitsky, N.A. Kuznetsova, O.A. Yuzhakova, V.M. Negrimovsky, A. B. Rubin, Biochemistry 74 (2010) 1305.
[22] D.M.G.C. Rocha, N. Venkatramaiah, M.C. Gomes, A. Almeida, Maria A.F. Faustino, Filipe A. Almeida Paz, Â. Cunha, João P.C. Tomé, Photodynamic inactivation of Escherichia coli with cationic ammonium Zn(ii) phthalocyanines, Photochem. Photobiol. Sci. 14 (2015) 1872.
[23] S. Tuncel, J. Fournier-dit-Chabert, F. Albrieux, V. Ahsen, S. Ducki, F. Dumoulin, Towards dual photodynamic and antiangiogenic agents: design and synthesis of a phthalocyanine-chalcone conjugate, Org. Biomol. Chem. 10 (2012) 1154–1157.
[24] F. Aribi, C. Vey, D. Topkaya, S.T. Kostakoglu, J. Fournier-dit-Chabert, S. I. Büyükekşi, G.C. Taşkın, S. Alpugan, F. Albrieux, A.G. Gürek, M. Cucca, K. Bennis, D. Atilla, V. Ahsen, S. Ducki, F. Dumoulin, Phthalocyanine-chalcone conjugates, J. Porphyrins Phthalocyan. 20 (2016) 497–504.
[25] H. Karaca, Z. Kurt, S. Sezer, Spectroelectrochemistry and catalytic Oxidation of 2-mercaptoethanol, J. Turkish Chem. Soc.: A 5 (2018) 701–718.
[26] H. Karaca, I. Şişman, E. Güzel, S. Sezer, F. Selimoğlu, B. Ergezen, M. Karaca, V. Eyüpoğlu, Thiochalcone substituted phthalocyanines for dye-sensitized solar cells: relation of optical and electrochemical properties for cell performance, J. Coord. Chem. 71 (2018) 1606–1622, https://doi.org/10.1080/00958972.2018.1468027.
[27] M. Xu, P. Wu, F. Shen, J. Ji, K.P. Rakesh, Chalcone derivatives and their antibacterial activities, Curr. Dev. Bioorg. Chem. 91 (2019), 103133.
[28] A. Elbourne, V.K. Truong, S. Cheeseman, P. Rajapaksha, S. Gangadoo, J. Chapman, R.J. Crawford, The use of nanomaterials for the mitigation of pathogenic biofilm formation, Methods Microbiol. 46 (2019) 61–92.
[29] P. Sen, A. Sindelo, D.M. Mafukidze, T. Nyokong, Synthesis and photophysicochemical properties of novel axially disubstituted silicon (IV) phthalocyanines and their photodynamic antimicrobial chemotherapy (PACT) activity against Staphylococcus aureus, Synth. Met. 258 (2019), 116203.
[30] R. Matshitse, M. Managa, T. Nyokong, The modulation of the photophysical and photodynamic therapy activities of a phthalocyanine by detonation nanodiamonds: comparison with graphene quantum dots and carbon nanodots, Diam. Relat. Mater. 101 (2020), 107617.
[31] A. Ogunsipe, J.Y. Chen, T. Nyokong, Photophysical studies of zinc (II) phthalocyanine-effects of substituents and solvents, New J. Chem. 28 (2004) 822–827.
[32] T. Nyokong, E. Antunes, in: K.M. Kadish, K.M. Smith, R. Guilard (Eds.), The Handbook of Porphyrin Science. World Scientific, Singapore, 2010, pp. 247–349.
[33] O.L. Osifeko, M. Dormus, T. Nyokong, Physicochemical and photodynamic antimicrobial chemotherapy studies of mono- and tetra-pyridyloxy substituted indium (III) phthalocyanines, J. Photochem. Photobiol. A 301 (2015) 47–54.
[34] Y.I. Openda, P. Sen, M. Managa, T. Nyokong, Acetophenone substituted phthalocyanines and their graphene quantum dots conjugates as photosensitizers for photodynamic antimicrobial chemotherapy against Staphylococcus aureus, Photodiagn. Photodyn. Ther. 29 (2020) 101607–101617.
[35] A. Magadla, D.O. Olowole, M. Managa, T. Nyokong, Physicochemical and antimicrobial photodynamic chemotherapy (against E. coli) by indium phthalocyanines in the presence of silver-iron bimetallic nanoparticles, Polyhedron 162 (2019) 30–36.
[36] L.J. Tavaresa, E.D. de Avilaa, M.I. Kleina, B.H.D. Panariello, D.M.P. Spolidórioc, A. C. Pavarinaa, Antimicrobial photodynamic therapy alone or in combination with antibiotic local administration against biofilms of Fusobacterium nucleatum and Porphyromonas gingivalis, J. Photochem. Photobiol. B 188 (2018) 135–145.
[37] J. Tan, Z. Liu, Y. Sun, L. Yang, L. Gao, Inhibitory effects of photodynamic inactivation on planktonic cells and biofilms of Candida auris, Mycopathologia 184 (2019) 525–531, https://doi.org/10.1007/s11046-019-00352-9.
[38] S. Shenvi, K. Kumar, K.S. Hatti, K. Rijesh, L. Diwakar, G. Chandrasekara Reddy, Synthesis, anticancer and antioxidant activities of 2, 4, 5-trimethoxy chalcones and analogues from asaronaldehyde: structureeactivity relationship, Eur. J. Med. Chem. 62 (2013) 435–442.

[39] L. Özdemir, Y. Yılmaz, M. Sönmez, M. Akkurt, M.N. Tahir, Synthesis and crystal structure of a new phthalonitrile and its phthalocyanines bearing diamagnetic metals, synthesis and reactivity in inorganic, metal-organic, Nano-Metal Chem. 46 (2016) 110–117.
[40] Y. Rio, M.S. Rodrıguez-Morgade, T. Torres, Modulating the electronic properties of porphyrinoids: a voyage from the violet to the infrared regions of the electromagnetic spectrum, Org. Biomol. Chem. 6 (2008) 1877–1894.
[41] E. Gürel, M. Pişkin, S. Altun, Z. Odabaş, M. Durmuş, Synthesis, characterization and investigation of the photophysical and photochemical properties of highly soluble novel metal-free, zinc(II), and indium(III) phthalocyanines substituted with 2,3,6-trimethylphenoxy moieties, Dalton Trans. 44 (2015) 6202–6211.
[42] M. Durmus, V. Ahsen, Water-soluble cationic gallium (III) and indium (III) phthalocyanines for photodynamic therapy, J. Inorg. Biochem. 104 (2010) 297–309.
[43] A.V. Zasedatelev, T.V. Dubinina, D.M. Krichevsky, V.I. Krasovskii, V.Y. Gak, V. E. Pushkarev, L.G. Tomilova, A.A. Chistyakov, Plasmon-induced light absorption of phthalocyanine layer in hybrid nanoparticles: enhancement factor and effective spectra, J. Phys. Chem. C 120 (2016) 1816–1823.
[44] L. Li, J.F. Zhao, N. Won, H. Jin, S. Kim, J.Y. Chen, Quantum dot-aluminum phthalocyanine conjugates perform photodynamic reactions to kill cancer cells via fluorescence resonance energy transfer, Nanosc. Res. Lett. 7 (2012) 386–393.
[45] X.F. Zhang, S.P. Liu, X.N. Shao, Noncovalent binding of xanthene and phthalocyanine dyes with graphene sheets: the effect of the molecular structure revealed by a photophysical study, Spectrochim. Acta Part A: Mol. Biomol. Spect. 113 (2013) 92–99.
[46] W. Shi, H. Fan, S. Ai, L. Zhu, Preparation of fluorescent graphene quantum dots from humic acid for bioimaging application, New J. Chem. 39 (2015) 7054–7059.
[47] J. Wu, P. Wang, F. Wang, Y. Fang, Investigation of the microstructures of graphene quantum dots (GQDs) by surface-enhanced Raman spectroscopy, Nanomaterials 8 (2018) 864–874.
[48] Z. Li, C. He, Z. Wang, Y. Gao, Y. Dong, C. Zhao, Z. Chen, Y. Wu, W. Song, An ethylenediamine-modified graphene oxide covalently functionalized with tetracarboxylic Zn(II) phthalocyanine hybrid for enhanced nonlinear optical properties, Photochem. Photobiol. Sci. 15 (2016) 910–919.
[49] T. Palaniselvam, H. Barike Aiyappa, S. Kurungot, An efficient oxygen reduction electrocatalyst from graphene by simultaneously generating pores and nitrogen doped active sites, J. Mater. Chem. 22 (2012) 23799.
[50] M. Miletin, P. Zimcik, V. Novakova, Photodynamic properties of aza-analogues of phthalocyanines, Photochem. Photobiol. Sci. 17 (2018) 1749–1766.
[51] T. Nyokong, Effects of substituents on the photochemical and photophysical properties of main group metal phthalocyanines, Coord. Chem. Rev. 251 (2007) 1707–1722.
[52] T.G.B. de Souza, M.G. Vivas, C.R. Mendonça, S. Plunkett, M.A. Filatov, M.O. Senge, L. De Boni, Studying the intersystem crossing rate and triplet quantum yield of meso-substituted porphyrins by means of pulse train fluorescence technique, J. Porphyrins Phthalocyan. 20 (2016) 282–291.
[53] M.Y. Berezin, S. Achilefu, Fluorescence lifetime measurements and biological imaging, Chem. Rev. 110 (2010) 2641–2684, https://doi.org/10.1021/cr900343z.
[54] V. Çakır, M. Goksel, M. Durmus, Z. Biyiklioglu, Synthesis and photophysicochemical properties of novel water soluble phthalocyanines, Dye. Pigment. 125 (2016) 414–425.
[55] A. Kelarakis, From highly graphitic to amorphous carbon dots: a critical review, MRS Energy Sustain. 1 (2014) 1–15, https://doi.org/10.1557/mre.2014.7.
[56] N. Maldonado-Carmona, T.S. Ouk, M.J.F. Calvete, M.M. Pereira, N. Villandiera, S. Leroy-Lhez, Conjugating biomaterials with photosensitizers: advances and perspectives for photodynamic antimicrobial chemotherapy, Photochem. Photobiol. Sci. 19 (2020) 445.
[57] T. Dai, B.B. Fuchs, J.J. Coleman, R.A. Prates, C. Astrakas, T.G. St Denis, M. S. Ribeiro, E. Mylonakis, M.R. Hamblin, George P. Tegos, Concepts and principles of photodynamic therapy as an alternative antifungal discovery platform, Front. Microbiol. 3 (2012), https://doi.org/10.3389/fmicb.2012.00120, 1–1.
[58] L.M. Tokubo, P.L. Rosalen, J. de Cássia Orlandi Sardi, I.A. Freires, M. Fujimaki, J. E. Umeda, P.M. Barbosa, G.O. Tecchio, N. Hioka, C.F. de Freitas, R.S.S. Terada, Antimicrobial effect of photodynamic therapy using erythrosine/methylene blue combination on Streptococcus mutans biofilm, Photodiagn. Photodyn. Ther. 23 (2018) 94–98.
[59] R.F. Donnelly, P.A. McCarron, M.M. Tunney, A.D. Woolfson, Potential of photodynamic therapy in treatment of fungal infections of the mouth. Design and characterisation of a mucoadhesive patch containing toluidine blue, J. Photochem. Photobiol. B 86 (2007) 59–69, https://doi.org/10.1016/j.jphotobiol.2006.07.011.
[60] Q. Deng, P. Sun, L. Zhang, Z. Liu, H. Wang, J. Ren, X. Qu, Porphyrin MOF dots-based, function-adaptive nanoplatform for enhanced penetration and photodynamic eradication of bacterial biofilms, Adv. Funct. Mater. 29 (2019) 1903018–1903027, https://doi.org/10.1002/adfm.201903018.
[61] A.P. Ribeiro, M.C. Andrade, F. da Silva Jde, J.H. Jorge, F.L. Primo, A.C. Tedesco, et al., Photodynamic inactivation of planktonic cultures and biofilms of Candida albicans mediated by aluminum-chloride-phthalocyanine entrapped in nanoemulsions, Photochem. Photobiol. 89 (2013) 111–119, https://doi.org/10.1111/j.1751-1097.2012.01198.x.
[62] I.B. Rosseti, L.R. Chagas, M.S. Costa, Photodynamic antimicrobial chemotherapy (PACT) inhibits biofilm formation by Candida albicans, increasing both ROS production and membrane permeability, Lasers Med. Sci. 29 (2014) 1059–1064, https://doi.org/10.1007/s10103-013-1473-4.